High-throughput estimation of incident light, light interception and radiation-use efficiency of thousands of plants in a phenotyping platform

Llorenç Cabrera-Bosquet, Christian Fournier, Nicolas Brichet, Claude Welcker, Benoît Suard, François Tardieu

METHODS PAPER

High throughput estimation of incident light, light interception and radiation-use efficiency of thousands of plants in a phenotyping platform

Llorenç Cabrera-Bosquet, Christian Fournier, Nicolas Brichet, Claude Welcker, Benoît Suard & François Tardieu

UMR LEPSE, INRA, Montpellier SupAgro, 34000, Montpellier, France

Author for correspondence:
Llorenç Cabrera-Bosquet, Tel. : +33 499 612 956, Fax: +33 467 612 116,
Email: llorenc.cabrera@supagro.inra.fr

Total word count (excluding summary, references and legends):	6252	No. of figures:	9
Summary	199	No. of tables:	0
Introduction	853	No of Supporting Information files:	5 (Fig. S1-2, Table S1, Methods S1, Video S1)
Material and Methods	1941		
Results:	1726		
Discussion:	1732		
Acknowledgements:	96		

Running title: High-throughput evaluation of light interception and radiation-use efficiency

This is a pdf file of an unedited manuscript that has been accepted for publication in New Phytologist. Please cite this article with its DOI: 10.1111/nph.14027

Summary

- Light interception and radiation use efficiency (RUE) are essential components of plant performance. Their genetic dissections require novel high-throughput phenotyping methods.
- We have developed a suite of methods to evaluate (i) the spatial distribution of incident light as experienced by hundreds of plants in a greenhouse, by simulating sun beam trajectories through greenhouse structures every day of the year (ii) the amount of light intercepted by maize (*Zea mays*) plants, via a functional-structural model using 3D reconstructions of each plant placed in a virtual scene reproducing the canopy in the greenhouse and (iii) RUE, as the ratio of plant biomass to intercepted light.
- The spatial variation of direct and diffuse incident light in the greenhouse (up to 24%) was correctly predicted at the single-plant scale. Light interception largely varied between maize lines that differed on leaf angles (nearly stable between experiments) and area (highly variable between experiments). Estimated RUEs varied between maize lines but were similar in two experiments with contrasting incident light. They closely correlated with measured gas exchanges.
- The methods proposed here identified reproducible traits that might be used in further field studies, thereby opening the way for large-scale genetic analyses of the components of plant performance.

Key words: environmental characterization, high-throughput phenotyping, maize, light interception, radiation-use efficiency, architecture

Introduction

Understanding the genetic controls of biomass production and yield is a major challenge in the context of climate change (Murchie *et al.*, 2009; Zhu *et al.*, 2010; Reynolds *et al.*, 2012). Yield (*Y*) can be dissected as a function of incident light (PPFD), the fraction of light intercepted by the crop (ε), the efficiency of the conversion of light into biomass, also called radiation-use efficiency (RUE,(Monteith, 1977)) and the partitioning of biomass to yield (harvest index, *HI*):

$$Y = HI \times \sum_{i=1}^{n} PPFD_i \times \varepsilon_i \times RUE_i, \quad (1)$$

where *n* is the duration of crop growth (d), $PPFD_i$, ε_i and RUE_i are the incident light, the fraction of intercepted light and RUE on the i^{th} day. *Y* can be genetically improved by increasing any of the terms of Eq. 1. Whereas *HI* has been one of the main determinants for improving yields in wheat during the 20th century (Calderini *et al.*, 1995; Sayre *et al.*, 1997), there is probably little avenue for further improvements in most crops (Austin *et al.*, 1980; Foulkes *et al.*, 2011; Reynolds *et al.*, 2012). The remaining terms of Eq. 1, ε and RUE, are directly related to light capture and photosynthetic efficiency at canopy level (Zhu *et al.*, 2010; Reynolds *et al.*, 2012). The genetic variability of leaf area development has a high effect on light interception at early stages of the plant cycle (Hay & Porter, 2006; Murchie *et al.*, 2009). Changes in canopy architecture also affect interception *via* genotypes with erect leaves that decrease light saturation at the top of the canopy and allow better penetration of light, thereby reducing the proportion of leaf area experiencing low light (Long *et al.*, 2006; Zhu *et al.*, 2010; Reynolds *et al.*, 2012). Studies comparing the relationship between the genetic variabilities of leaf architecture and light interception at the intraspecific level have been limited to a small number of genotypes, with contrasting conclusions (Louarn *et al.*, 2008; Hammer *et al.*, 2009; Moreau *et al.*, 2012).

Estimations of RUE are usually based on consecutive and destructive sampling of aboveground biomass over time, which is not feasible for the large number of genotypes involved in genetic analyses (Sinclair & Muchow, 1999). Gas-exchange measurements are also difficult to tackle at high throughput and are usually limited to measurements at the single-leaf level (Albrizio & Steduto, 2005). A phenotyping platform allowing measurements of 3D plant architecture and estimates of plant biomass with a time definition of one day

offers new possibilities to estimate light interception and RUE of hundreds of genotypes, together with their responses to environmental conditions. However, no method is currently proposed because of technical difficulties.

- The spatial variability of incident light can be up to 30% within a greenhouse (Stanhill *et al.*, 1973; Kozai & Kimura, 1977; Brien *et al.*, 2013) or a growth chamber (Granier *et al.*, 2006). Conditions also vary between experiments, in greenhouses because of climatic conditions and in growth chambers because of differences between chambers (Massonnet *et al.*, 2010). A genetic analysis of plant performance therefore requires a precise evaluation of the PPFD (diffuse and direct) available to each plant of the greenhouse or growth chamber during each experiment.

- Light interception can be derived from 3D plant architecture, combined with estimates of the direction of sunbeams and with the proportion of direct *vs*. diffuse light (Sinoquet *et al.*, 2001). Platform experiments present a difficulty compared with the field, namely that they often harbour composite canopies in which each plant is surrounded by plants of another genotype. Hence, it is necessary to distinguish the light interception by each plant to dissect the genetic variabilities of ε and RUE.

The objective of this paper was to develop a non-invasive, automatized and accurate procedure to derive light interception and radiation-use efficiency in high-throughput phenotyping platforms. To our knowledge, we present here the first methods for estimating the local PPFD received by each individual plant and for estimating light interception and RUE at a throughput of thousands of plants. We have tested whether RUE derived from the methods presented here is stable between experiments and related to leaf gas-exchange measurements.

Material & Methods

The PHENOARCH phenotyping platform

The PHENOARCH platform (http://bioweb.supagro.inra.fr/phenoarch), hosted at the M3P, Montpellier Plant Phenotyping Platforms (https://www6.montpellier.inra.fr/lepse/M3P), is based on a PhenoWare™ system (PhenoWare™, Lyon, France) composed of a conveyor belt structure of 28 lanes carrying 60 carts with one pot each (i.e. 1680 pots), plus a conveyor belt system that feeds the imaging or the watering units. The imaging unit is composed of two cabins with 3D image acquisition involving top and side RGB cameras (Grasshopper3, Point Grey Research, Richmond, BC, Canada) equipped with 12.5-75mm TV zoom lens (Pentax, Ricoh Imaging, France) and LED illumination (5050 - 6500K colour temperature). Five watering units are composed of weighing terminals (ST-Ex, Bizerba, Balingen, Germany) and high-precision pumps (520U, Watson Marlow, Wilmington, MA, USA). Circulation of plants through conveyors, image acquisition and irrigation management are controlled by an industrial open automation system based on PC Control technology (Beckhoff CX 2020, Beckhoff Automation, Verl, Germany) that allows localization in real time of every pot in the platform and individually programming pot displacements. Imaging and watering routines are sequentially performed every day. Plants are then moved back to the same positions and orientation, so plant position in respect to neighbours is conserved throughout the experiment. PHENOARCH has held experiments with different species including cereals (maize (*Zea mays* L.), wheat, rice, sorghum) (Sciara *et al.*, 2015), grapevine (Coupel-Ledru *et al.*, 2014) and apple trees (Lopez *et al.*, 2015). The plant density can be adapted for each species, from 13 plants m^{-2} in the default setting with 1680 plants to double densities for smaller plants or half densities for small trees or adult maize plants. Experiments performed until mid-2014 used a Lemnatec technology (LemnaTec, Wüerselen, Germany) that was then replaced by the methods presented above.

Micro-meteorological conditions are constantly monitored at six positions in the greenhouse at the top of the plant canopy. Air temperature and humidity are measured every minute (HMP45C, Vaisala Oy, Helsinki, Finland), together with PPFD (SKP215, Skye Instruments, Powys, UK). The temperature of the meristematic zone of eight plants distributed in the greenhouse is measured with a fine copper-constantan thermocouple (0.2 mm diameter) located between the sheaths of two leaves located at meristem height. Air vapour pressure

difference (VPD) is estimated at each time step as the difference in water vapour pressure between saturation at air temperature and the current vapour pressure in the air. All data of air/meristem temperature, PPFD and relative humidity are averaged and recorded every 15 min (NI CompactRio, National Instruments, Austin, TX, USA) and stored in the PHIS database (http://web.supagro.inra.fr/phis).

Spatial variability of incident light in the greenhouse

Daily incident PPFD over each plant of the platform ($PPFD_{(xy)}$) was estimated by combining a 2D map of light transmission and the outside PPFD ($PPFD_{ext}$) measured every 15 min with a sensor placed on the greenhouse roof (SKS 1110, Skye Instruments, Powys, UK). Maps of the fraction of transmitted direct (T_{dir}) and diffuse (T_{dif}) light were calculated every hour of each day of the year by using 169 hemispherical images of the greenhouse using a digital camera (Nikon Coolpix 4500, Nikon, Melville, NY, USA) fitted with a fisheye lens with a 183° field of view (Nikon FC-E8 Fisheye Converter, Nikon). Images were taken every m^2 in the greenhouse, at 0.4, 1 and 1.5 m high, i.e. at heights representing the top of canopies of different species and phenological stages. Only data at 1m height are presented here. The camera and lens were placed vertically (checked with a spirit level) and the geographical North was referenced. Hemispherical images were analysed using the Ilastik 1.1.8 software (Sommer *et al.*, 2011) (Supporting Information Fig. S1, Table S1). Calculation of sun paths, transmitted direct and diffuse radiation was then performed using standard astronomical formulae using R scripts (R_Core_Team, 2015) available as an open application (Supporting Information Methods S1). The refraction in the glass of the greenhouse changed the angle of sun beams by 0 to 36° for incident angles up to 60°. It returned to its original value in air so refraction resulted in a translation of sunbeams by 0 to 2 cm, and was therefore considered as negligible. The amount of transmitted direct radiation was computed every hour as a function of solar position, calculated from the daily time-course of sun path, in relation to the gap fraction at each position along the sun path (i.e. fraction of the image without greenhouse structure or lamps, Fig. 1). The amount of transmitted diffuse PPFD was calculated using a standard overcast sky (SOC) diffuse model (Moon & Spencer, 1942), in which diffuse radiation flux varies with zenith angle and then depends on the gap fraction of the greenhouse. Transmissions of direct and diffuse light were further corrected by the

transmittance coefficient of light through glass, measured using a spectroradiometer (HR4000, Ocean Optics, Dunedin, FL, USA).

The amount of PPFD reaching each of the XY positions within the greenhouse ($PPFD_{(x,y)}$) on a given day (i) was calculated as:

$$PPFD_{(x,y)i} = \sum_{j=0}^{d} f_{d,j} \times PPFD_{ext,j} \times T_{dir(x,y)j} + (1 - f_{d,j}) \times PPFD_{ext,j} \times T_{dif(x,y)} \quad (2)$$

Where f_d is the fraction of direct light and (1- f_d) is the fraction of diffuse light from incoming external global radiation corresponding to the j^{th} hour and d the duration of daylight, calculated according equations detailed in (Spitters *et al.*, 1986).

Image analysis and reconstruction of plant architecture

RGB colour images (2056 x 2454) from thirteen views (twelve side views from 30° rotational difference and one top view) were captured daily for each plant during the night. Images were captured while the plant was slowly rotating using a brushless motor. Top and side cameras were calibrated using reference objects in order to convert pixels into mm^2. Plant pixels from each image were segmented from those of the background with HSV thresholding using OpenCV libraries (Open Source Computer Vision Library: http://opencv.org). A 3D representation of each plant of the platform was obtained using a silhouette-carving algorithm. Plant skeletons were extracted from binarised 2D RGB images using the thinning algorithm of (Zhang & Suen, 1984), implemented in ImageJ (Rasband, 1997-2014). Skeletons were further processed with the 'Analyse Skeleton' ImageJ plugin (Arganda-Carreras *et al.*, 2010) to obtain crossings and the endpoints of the different branches of the skeleton. These points were used to navigate through the skeleton image and segment it into 50-pixels-long elementary lines. The angle of each elementary segment with the vertical was computed as the absolute value of the arctangent between z- and x-coordinates of segments endpoints. All data, namely raw and processed images together with metadata were stored in the PHIS database (http://web.supagro.inra.fr/phis/).

Light interception and radiation-use efficiency

Daily light interception was estimated for each plant of the platform by using the functional-structural RATP (radiation absorption, transpiration and photosynthesis) plant model (Sinoquet *et al.*, 2001) available under OpenAlea platform (http://openalea.gforge.inria.fr/dokuwiki/doku.php) (Pradal *et al.*, 2008; Pradal *et al.*, 2015).

Briefly, the canopy was split into cubic voxels of 0.2 m, characterized each by the density of leaf area and the leaf angle distribution calculated from the 3D virtual representations of the neighbouring plants. Density of leaf area was calculated as the cumulative area of all leaf segments in the voxel, regardless of the plant they originated from. The calculated mean leaf angle in a voxel was calculated as the mean of angles of all leaf segments in the considered voxel.

For each voxel, intercepted PPFD was calculated every day from a sample of 46 beam angles, with a cumulative value equal to the incident PPFD at the corresponding x y position in the greenhouse ($PPFD_{(xy)}$). For each direction, beam extinction was computed by applying Beer's law within the sequence of intersected cells by each beam. The daily PPFD intercepted by each plant was obtained by cumulating the PPFD interception for each voxel weighed by the relative contribution of the considered plant to the voxel area. Radiation-use efficiency was then estimated as the slope of plant biomass production to cumulative intercepted PPFD.

Leaf gas exchange measurements

A portable open gas exchange system (LI-COR 6400XT, LI-COR Inc., Lincoln, NE, USA) was used to measure leaf gas exchange in youngest fully expanded leaf blades in a set of eight maize lines. The net CO_2 assimilation rate (A_N), stomatal conductance (g_s) of those leaves were measured inside the greenhouse from 10:00 to 14:00 (solar time) at 1500 µmol photon m^{-2} s^{-1} of PPFD, a leaf temperature of 28ºC, a leaf-to-air vapour pressure deficit of about 1.2-1.5 kPa and an ambient CO_2 of 400 µmol mol^{-1}.

Plant growth

The leaf area and the fresh plant weight of individual plants were estimated from images taken in 13 directions. Briefly, pixels extracted from RGB images were converted into fresh plant weight and leaf area using linear models derived from regression of data from multiple side view images and destructive measurements performed at different phenological stages, from 5 to 14 appeared leaves (i.e. from 15 to 50 days at 20°C after emergence). The resulting conversion was accurate and unbiased (Supporting Information Fig. S2). The time courses of leaf area or fresh plant weight were then fitted individually to the three-parameter Gompertz function,

$$y = a \times e^{-e^{(b-cx)}} \quad (3)$$

using appropriate R scripts (R_Core_Team, 2015). Time courses were expressed as a function of equivalent days at 20°C (Parent *et al.*, 2010). At the end of the experiment, shoots of all plants were harvested and total plant biomass was measured.

Genetic material and growth conditions

The techniques presented above were tested in two experiments carried out in autumn (Exp. 1) and winter-spring (Exp. 2), with markedly different incident PPFD. Two panels were studied involving 60 and 200 maize (*Zea mays* L.) lines for Exp. 1 and Exp. 2, respectively. A common set of 23 maize inbred lines with tropical origin was grown in both experiments, chosen for maximising the genetic and phenotypic variabilities. Plants were grown in polyvinyl chloride (PVC) 9 L pots (0.19 m diameter, 0.4 m high) filled with a 30:70 (v/v) mixture of a clay and organic compost. Three seeds per pot were sown at 0.025m depth and thinned to one per pot when leaf three emerged. In each of the experiments two levels of soil water content were experienced; (i) retention capacity (WW, soil water potential of -0.05 MPa) and (ii) mild water deficit (WD, soil water potential of -0.5 MPa) by compensating transpired water three times per day via individual measurements of each plant. The weight of water in each pot was calculated at the beginning of the experiment from the weight of soil and measured soil water content. It was then maintained at a constant value by considering that the weight loss between two time-points was due to transpiration plus soil evaporation, after correction for the change in plant fresh weight every day (Eq. 3). Each line was replicated 5 and 7 times for the WW and WD treatments, respectively in Exp. 1, whereas each line was replicate 4 times in Exp. 2. Greenhouse temperature was maintained at 25 ± 3°C during the day and 20°C during the night. Supplemental light was provided either during day time when external solar radiation dropped below 300 W m^{-2} or to extend photoperiod using 400 W HPS Plantastar lamps (OSRAM, Munich, Germany) with 0.4 lamps m^{-2}. The resulting photoperiod was 12/12h day/night. The amount of light supplied by lamps was taken into account in the calculations of local PPFD.

Statistical analyses

Two-way analyses of variance (ANOVA) were performed using the lm procedure (R_Core_Team, 2015) to calculate the effects of experiment and genotype. Broad-sense heritability (h^2) was calculated as:

$$h^2 = \sigma^2_G / (\sigma^2_G + \sigma^2_e/r) \quad (4)$$

Where σ^2_G is the genotypic variance, σ^2_e is the residual variance, and r is the number of plant replicates per genotype. All statistical tests and graphs were performed using R 3.1.3 (R_Core_Team, 2015).

Results

Estimating the spatial variability of local available light for each plant of the platform

We have modelled the fraction of direct and diffuse light reaching each plant every hour of each day of the year based on 169 hemispherical images taken at different x-y positions of the greenhouse (1 image m^{-2}), which capture the obstacles to light (e.g. beams of the greenhouse, lamps or cabins, Fig. 1). For each image, the daily time-course of sun path was simulated based on the latitude, day of year and time of day, as presented in Fig. 1a-d for summer and winter solstices and spring and autumn equinoxes. Sun paths occupied more central positions in the image and were longer during summer compared to winter because of the changes of solar position with the vertical. They crossed the structures of the greenhouse for a fraction of the day and reached plants (path superimposed on the sky) otherwise. The proportion of transmitted direct PPFD was estimated from the gap fraction over the sun path (frequency for a light beam to cross the structure in the absence of obstacle), weighed for light intensity and displacement rate along the sun path at each time-step (Supporting Information, Methods S1). Light transmission through the greenhouse glass was also estimated, resulting in a transmittance coefficient (k_g) of 0.76.

Daily transmission of direct light was calculated every day for each of the 1680 positions in the greenhouse, resulting in large spatial and temporal variations. The duration of peaks of transmission was shorter in winter than in summer solstices, whereas the maximum value was close to 60% in all cases (Fig. 1e-h). The time course of transmission also changed with position in the greenhouse (Fig. 1e-l), with a spatial variability that was greater in winter, with up to 30% differences between locations, compared to 14% in summer. The x-y position with maximum transmission itself changed with time of year. Integrated over one day, these data resulted in a map of direct transmission for each day of the year (Fig. 2i-l, Supporting Information Video S1). The transmission of diffuse radiation was also calculated for each position of the greenhouse from the same hemispherical images, resulting in a spatial variation of 11.9% (Fig. 2b). Whereas transmission of direct light maps was calculated each

281 day of the year (Fig. 2a), the transmission of diffuse light only depends of the greenhouse
282 structure so the map presented in Fig 2b is independent of days of the year. The total
283 amount of direct plus diffuse PPFD reaching each location in the greenhouse was finally
284 estimated using Eq. 2 (Fig. 2).

285 The method presented above can be extended to any other greenhouse provided that
286 images are available (Supplementary Information Methods S1). It was tested by comparing
287 the simulated PPFD at six locations in the greenhouse with PPFD measured at the same
288 locations. Measured PPFD cumulated over one week showed an appreciable spatial
289 variability (24%, from 173 to 220 mol m^{-2}), which was adequately accounted for by the
290 simulated PPFD at the same positions (Fig. 3a). The daily time courses of observed vs
291 simulated PPFD averaged over the six positions in the greenhouse were also compared on
292 two days with high and low PPFD values, respectively. Fig. 3b shows that observed and
293 simulated time courses closely matched, so the cumulative PPFD values estimated with the
294 methods presented above was not biased.

295 ***Estimating leaf angles over time***

296 The side plant image containing maximum information for the quantification of leaf angles
297 was chosen for each plant and day as that containing most leaves (Fig. 4a). To that end, we
298 have used the binarised top view of the plant on which we performed a reduced major axis
299 regression, allowing us to choose the side image with the best angle (Fig. 4b). This image was
300 then segmented and skeletonized (Fig. 4cd). The endpoints of the different branches of plant
301 skeletons (red circles) were used to navigate through the skeleton and to dissect it into 50-
302 pixels-long elementary segments (Fig. 4f). The orientation of each elementary segment was
303 then computed, thereby allowing calculation of angles for each segment. The mean leaf
304 angle was then computed either for a whole plant or in each voxel, as shown in Fig. 4e for
305 the plant presented in Fig 4a-e. An example of this procedure is shown in Figure 4g where
306 mean leaf angles clearly differed between three maize lines showing either sub-horizontal
307 angles (close to 0) or more erect architectures. Angles corresponding to each line remained
308 essentially stable with phenological stages as illustrated in Figure 4h.

309 ***Calculating daily light interception by each plant of the greenhouse***

310 The composite canopy in the greenhouse (i.e. with neighbouring plants belonging to
311 different lines) was reconstructed from individual 3D point cloud representations of each

plant, and split into in a grid of voxels for calculating light interception using the RATP model. For each plant, actual plant leaf area and plant leaf angle distribution were uniformly distributed among the 3D point cloud. Figure 5 represents a schematic diagram of how the RATP modelling inputs were generated:

- First, reconstructed 3D plants were positioned according to their actual coordinates in the greenhouse to obtain a 3D point cloud representing the canopy (Fig 5a).
- Second, a 3D grid with cubic voxels of 0.20 m side was fit to the canopy bounding box and filled using positions, leaf angles and leaf areas associated to each point of the 3D canopy (Fig. 5a). Each voxel may thus include leaves of several neighbouring plants, with a range of angular distribution. Fig. 5b represents the whole greenhouse discretized in this way, where represented volumes are proportional to the leaf area in the corresponding voxel and the colour represents the dominant leaf angle.
- Fourth, intercepted PPFD was calculated every day in each voxel from local $PPFD_{(xy)i}$ obtained with light maps. The calculation began with upper voxels, so the light reaching voxels at lower positions depended on both local PPFD and on transmission through upper voxels. The amount of PPFD intercepted by each voxel was then partitioned between neighbouring plants as a proportion of leaf area of each plant in the considered voxel.
- Finally, the daily PPFD intercepted by each plant was computed by cumulating PPFD intercepted by this plant by each voxel.

An example of reconstructed architecture of ten neighbouring plants and of calculated intercepted PPFD is presented in Fig. 6 at three times of the plant cycle (20, 35 and 50 d after sowing). Leaves increasingly interacted with each other on days 35 onwards (Fig. 6a-c). Calculated intercepted light (Fig 6d-f) increased with time, with an increasing variability between plants. The model captured (i) the effect of architectural characteristics of each plant on days 20 and 35 (see the comparison between plants 6, 7 and 10 with low angles with horizontal, *vs*. plant 2 with higher angle), (ii) the competition between plants on day 50, in which tall plants such as plant 2 had a much higher light interception compared with smaller, dominated plants such as plant 3. Hence, light interception on days 20 and 35 might be considered as similar to those of plants in a canopy with a single genotype, while that on day 50 largely depended on the spatial distribution of different genotypes in the greenhouse.

The suite of methods presented here allowed unifying experiments carried out in different seasons, with a common ranking of genotypes for radiation-use efficiency.

We have tested the interest of the method in an experiment with 200 maize lines and by comparing a set of 23 maize lines in two experiments. The latter were performed at contrasting incident PPFDs in order to compare values of RUE. Overall, plants accumulated more biomass in winter/spring compared to autumn (75%, Fig. 7a), with a correlation between genotype performance in autumn and spring, although the ranking of genotypes slightly changed between experiments (genotype x environment interaction, Fig. 7a inset). Light interception also clearly differed between experiments, largely due to a difference in leaf area (55% difference, not shown). In contrast, the relation between intercepted light and biomass was common to both experiments (Fig. 7e). Indeed, the difference in biomass between experiments was entirely accounted for by the difference in intercepted light (12.5 and 23 mol plant^{-1} in autumn and winter/spring, respectively, Fig. 7b), attributable to higher leaf area development and higher amount of incident light. Hence, the mean RUE of the canopy (slope of the regression between biomass and intercepted PPFD) was common to both experiments. Furthermore, RUEs measured on individual lines closely correlated between the two experiments (Fig. 7f inset), with neither significant effects of experiment nor genotype x experiment interaction. The genotypic difference in RUE was significant, ranging from 7.0 to 11.1 g FW mol $^{-1}$. Hence, the methods presented here allowed dissecting the differences between two experiments with large differences in biomass into (i) genotypic traits that did not differ between experiments but had a high genetic variability, namely leaf angle and radiation-use efficiency, (ii) environmental differences, essentially incident light, that affected both biomass and leaf area, thereby generating the large differences that were observed between experiments, (iii) plant traits that differed between experiments due to environmental variables, in particular leaf growth.

We have extended our analysis in Exp. 2b to 1600 plants of 200 genotypes, subjected or not to a mild water deficit (Fig. 8). Overall, both biomass and light interception were affected by water deficit, with a high genetic variability in both cases. Estimated RUE had a large genetic variability (from 6.0 to 12 g FW mol $^{-1}$) and was affected by water deficit by 12% in average. Hence, the change in biomass with water deficit was related to both intercepted light due to

373 a lower leaf area and to decreased RUE. In both watering scenarios biomass and RUE
374 displayed high heretabilities (0.7< h^2 <0.8).

375 Finally, we have checked whether the observed differences in RUE between genotypes were
376 related to gas-exchange measurements. This was performed in the 8 genotypes with highest
377 contrasts in RUE in Exp. 1 under two contrasting water conditions. Tight correlations were
378 observed between whole-plant RUE values and single-leaf net photosynthesis (r^2 = 0.54, P =
379 0.001) and stomatal conductance (r^2 = 0.61, P <0.001) (Fig. 9), suggesting that RUE estimated
380 at high throughput with the suite of methods presented here could be a surrogate for gas-
381 exchange measurements and vice versa.

382

Discussion

A characterization of the light received by each plant based on a model rather than by increasing sensor number

Consistent with intuitive observations of shaded zones in a greenhouse, our study shows that steep gradients of light availability occur over distances smaller than 1m, resulting in differences in incident PPFD by up to 10% between neighbouring plants. Hence, we confirm the large spatial variability of light in greenhouses (Stanhill *et al.*, 1973; Kozai & Kimura, 1977), but also provide a method for mapping it with high spatial resolution. If characterized directly with sensors, this mapping would need at least one sensor per m^2, i.e. hundreds of sensors technically difficult to maintain and calibrate. The method presented here avoids this problem by accurately simulating the incident light received by each plant at any time of the year. It has the advantage of having a spatial definition of tens of centimetres and of estimating the respective amounts of direct and diffuse PPFD received by plants, which can bias the calculation of intercepted light because of the high proportion of diffuse light in greenhouses (Sinclair *et al.*, 1992; Sinclair & Muchow, 1999). Finally, this method is rapid (the time for taking the 169 images was 4 hours, and the computing time was less than 2 hours). It can be used in any greenhouse regardless of the presence of a phenotyping platform, and is valid as long as the structures of the greenhouse are not changed, and as obstacles to light do not change with time of the year (e.g. a deciduous tree near the greenhouse).

A striking result of our study was the relatively low fraction of total daily transmitted light (ca. 30%) compared with other studies that state light transmissions ranging between 0.46 and 0.84% (Niinemets & Keenan, 2012). This discrepancy is probably due to the fact that most of studies measuring light transmission in greenhouses report values based on midday measurements with sun beams close to the vertical, thereby overestimating transmission (Niinemets & Keenan, 2012) .

Dissecting biomass accumulation allows identification of components with high repeatability and genetic variation.

We have shown that coupling a 3D reconstruction method to a structure-function model together with a fine characterisation of environmental conditions allows estimation of light

interception and RUE of thousands of plants with good heritabilities. The suite of methods presented here allowed dissection of biomass into (i) traits that are repeatable between experiments such as RUE or leaf angles, which have a large genetic variability (Mickelson *et al.*, 2002; Tian *et al.*, 2011; Ku *et al.*, 2012) and can therefore be considered as intrinsic to each genotypes, (ii) traits that are highly dependent on environmental conditions such as the change with time of intercepted light.

In the results presented in this work, RUE values ranged from 7.0 to 11 g FW mol $^{-1}$. If expressed in a dry weight basis (considering an average water content of 90%) and per unit of light energy (MJ), our estimates range from 3 to 5 g DW MJ^{-1}. These RUE values, although relatively high compared with field measurements, are often reported in plants grown in controlled environments (Hammer & Vanderlip, 1989). This high estimates of RUE can be related to the high proportion of diffuse radiation inherent to greenhouses or chamber structures (Sinclair *et al.*, 1992; Sinclair & Muchow, 1999). In addition, the lower daily incident radiation in the greenhouse compared with the field may induce high values of RUE through a greater photosynthetic efficiency and compensation mechanisms (Baille *et al.*, 2006). RUE values observed in this work are in accordance with other studies in maize if expressed in a dry weight basis (Otegui *et al.*, 1995; Lindquist *et al.*, 2005; Louarn *et al.*, 2008; Rattalino Edreira & Otegui, 2012). Proper measurements of plant dry biomass would be needed to compare with available field data. Furthermore, partitioning of biomass to roots and maintenance costs associated to respiration can be an important source of variation in RUE. Such measurements are not easily compatible with the throughput of 1680 plants presented in this study, so only the resulting RUEs can be estimated at this throughput.

Although genetic improvement of RUE has been suggested as a way to increase yield potential in major crops (Zhu *et al.*, 2010; Reynolds *et al.*, 2011), few studies have explored its genetic variability probably given to the technical difficulties to study this trait (Acreche *et al.*, 2009; Narayanan *et al.*, 2013; Koester *et al.*, 2016). Other works have shown the potential of 3D reconstruction methods coupled to light distribution algorithms (radiosity or ray tracing) to asses photosynthesis in plant canopies (Prieto *et al.*, 2012; Song *et al.*, 2013; Pound *et al.*, 2014; Burgess *et al.*, 2015). These methods rely on highly-realistic surface-

444 based plant reconstructions which require high number of images (ca. 35-65 per plant in
445 complex canopies) or plant digitisations that are difficult to automatize in the context of
446 high-throughput phenotyping. Conversely, our method, uses 3D point clouds that require
447 less reconstruction steps (i.e. binarisation and projection), is easy to automatize with
448 standard image analysis library (openCV), and can be obtained with a limited set of images
449 (from 3 to 12). Although precision in reconstruction is lower compared with the techniques
450 described above, our method can accommodate a certain level of error in the 3D
451 reconstructed plant provided that leaf area estimates are precise enough. Indeed, accurate
452 estimates of the total plant leaf area are easy to obtain from a set of binarised 2D images
453 (Supporting Information Fig. S2). (Golzarian *et al.*, 2011; Hartmann *et al.*, 2011). Another
454 advantage of RATP is that uses a statistical approach that avoids difficulties relating to
455 relative positions of leaves belonging to neighbouring plants. Indeed, the respective
456 positions of leaves may change from one day to another. This is the main reason why we
457 have adopted a probabilistic approach with the RATP model, rather than an explicit
458 description of beam intersecting virtual leaves.

459 The facts that RUE was highly heritable, repeatable between experiments with different
460 incident light (but similar soil water or nutrient status), and correlated with gas-exchange
461 measurements suggests that our measurement of RUE can have a great value for exploring
462 the genetic variability of a surrogate of canopy photosynthesis at high-throughput in large
463 collections of genotypes, which is a topic of growing interest (Slattery & Ort, 2015; Koester
464 *et al.*, 2016). This method may also allow exploring the change in RUE with environmental
465 conditions by subjecting collections of genotypes to a range of water or nitrogen status,
466 known to largely affect RUE (Teixeira *et al.*, 2014), of CO_2 concentration (Hui *et al.*, 2001;
467 Sakai *et al.*, 2006), or of temperature (Louarn *et al.*, 2008). Finally, using the genotypic values
468 of RUE estimated here in a crop model will allow examining its consequences on yield of a
469 large number of genotypes in a variety of climatic scenarios (Boote *et al.*, 2013; Parent &
470 Tardieu, 2014).

471 However, we are aware of several methodological difficulties associated with the approach
472 presented here. The first of them is that RUE is the result of a calculation that takes light
473 interception into account. Hence, any error in the estimation of intercepted light results in
474 an error in RUE. The method has been tested successfully in plants with relatively simple

475 architecture such as maize, but serious errors in the calculation of light interception can
476 occur in plants with complex architecture such as rapeseed, with a high level of occlusion
477 (i.e. in which many leaves are hidden by other leaves). The choice of voxel size can be
478 associated with inaccurate results (Combes *et al.*, 2008) and needs to be adjusted depending
479 on the species and the target variable of study. Indeed, it results from an optimization
480 between (i) an adequate representation of gaps in an open canopy and (ii) conforming to
481 Beer-Lambert assumptions within the voxel.
482
483 Other difficulties are associated with methodological choices. If the primary objective is to
484 analyse the genetic control of leaf growth and plant architecture, one tends to use images
485 taken during the night to minimize the change with time of leaf angles or shape due to
486 epinasty (Greenham *et al.*, 2015) or leaf rolling (Hay *et al.*, 2000; Sirault *et al.*, 2015),
487 especially under water deficit. However, this choice can bias the calculation of light
488 interception. Conversely, the use of day-time measurements results in more accurate
489 estimation of light interception but decrease the heritability of measurements of leaf area or
490 angles due to leaf movements or rolling during the day. In the same way, a full
491 characterization of light interception would require that plants are organized in micro-
492 canopies of about 10 plants sharing a common genotype. However, this considerably
493 decreases the number of genotypes studied per experiment, thereby impeding genome-
494 wide association studies that require at least 250-300 genotypes (Beavis, 1998; Malosetti *et*
495 *al.*, 2013). We show here that working with single plants surrounded by plants of different
496 genotypes can provide good results until plants of different genotypes shade each other (Fig.
497 7), but some traits such as the vertical distribution of light interception in the canopy cannot
498 be analysed with this design, although it can have an appreciable effect on light interception
499 (Moreau *et al.*, 2012; Sadras *et al.*, 2012). None of these points question the method itself,
500 but rather the protocol of the experiments using the method.
501 Whereas the method for light mapping can be easily applied in any greenhouse regardless of
502 the presence of a phenotyping platform, the light interception routine is only accessible to
503 platforms equipped with 3D imaging of individual plants, thereby limiting its diffusion. Its
504 main interest is to fill a gap in photosynthesis research, namely the high throughput
505 estimation of light interception and RUE in view of genetic analyses, rather than to be widely
506 distributed in hundreds of platforms.

Conclusion

We believe that the suite of methods proposed here may have a significant impact on future studies of canopy photosynthesis because of it is compatible with the necessary throughput for genetic analyses and because it allows dissecting the genetic variability of biomass accumulation into different traits that have each their genetic architecture. Field-estimations of intercepted light based on field-based imaging or spectral techniques (Comar *et al.*, 2012; Sankaran *et al.*, 2015) will still be necessary, but they can be combined with genotypic values of RUE and leaf angles estimated in the platform, thereby avoiding the time-consuming step of sequential destructive measurements of plant biomass.

Acknowledgements

This work was supported by the European Union Framework Program 7 'Drought-tolerant yielding plants' (DROPS) project (FP7-KBBE-244374) and the "*Infrastructure Biologie Santé*" Phenome supported by the National Research Agency and the "*Programme d'Investissements d'Avenir*" (PIA) (ANR-11-INBS-0012). Authors are grateful to Stéphane Berthézène, Antonin Grau, Jonathan Mineau, Vincent Nègre and Carine Palaffre, for their help in conducting the experiments. Simon Artzet is acknowledged for his help in constructing Figure 5. We thank Christophe Pradal and Marc Saudreau for the wrapping of RATP model on OpenAlea platform. We thank Tsu-Wei Chen for his critical comments on the manuscript.

Author Contributions

L. C-B., F.T. and C.W. planned and designed the research, L. C-B., B.S performed experiments, L. C-B., C.F. and N.B. analysed data and L. C-B., C.F. and F.T. wrote the manuscript.

References

Acreche MM, Briceno-Felix G, Martin Sanchez JA, Slafer GA. 2009. Radiation interception and use efficiency as affected by breeding in Mediterranean wheat. *Field Crops Research* **110**: 91-97.

Albrizio R, Steduto P. 2005. Resource use efficiency of field-grown sunflower, sorghum, wheat and chick-pea I. Radiation use efficiency. *Agricultural and Forest Meteorology* **130**: 254-268.

Arganda-Carreras I, Fernandez-Gonzalez R, Munoz-Barrutia A, Ortiz-De-Solorzano C. 2010. 3D Reconstruction of Histological Sections: Application to Mammary Gland Tissue. *Microscopy Research and Technique* **73**: 1019-1029.

Austin RB, Bingham J, Blackwell RD, Evans LT, Ford MA, Morgan CL, Taylor M. 1980. Genetic improvements in winter-wheat yields since 1900 and associated physiological-changes. *Journal of Agricultural Science* **94**: 675-689.

Baille A, Gutierrez Colomer RP, Gonzalez-Real MM. 2006. Analysis of intercepted radiation and dry matter accumulation in rose flower shoots. *Agricultural and Forest Meteorology* **137**: 68-80.

Beavis WD 1998. QTL analyses: power, precision, and accuracy. In: AH P ed. *Molecular Dissection of Complex Traits.* Boca Raton, Florida: CRC Press, 145-162.

Boote KJ, Jones JW, White JW, Asseng S, Lizaso JI. 2013. Putting mechanisms into crop production models. *Plant, Cell & Environment* **36**: 1658-1672.

Brien CJ, Berger B, Rabie H, Tester M. 2013. Accounting for variation in designing greenhouse experiments with special reference to greenhouses containing plants on conveyor systems. *Plant Methods* **9**: 5.

Burgess Aj, Retkute R, Pound MP, Preston SP, Pridmore TP, foulkes j, Jensen O, Murchie EH. 2015. High-resolution 3D structural data quantifies the impact of photoinhibition on long term carbon gain in wheat canopies in the field. *Plant Physiology* **169**: 1192-1204.

Calderini DF, Torresleon S, Slafer GA. 1995. Genetic-improvement in wheat yield and associated traits - a reexamination of previous results and the latest trends. *Annals of Botany* **76**: 315-322.

Comar A, Burger P, de Solan B, Baret F, Daumard F, Hanocq J-F. 2012. A semi-automatic system for high throughput phenotyping wheat cultivars in-field conditions: description and first results. *Functional Plant Biology* **39**: 914-924.

Combes D, Chelle M, Sinoquet H, Varlet-Grancher C. 2008. Evaluation of a turbid medium model to simulate light interception by walnut trees (hybrid NG38 x RA and *Juglans regia*) and sorghum canopies (*Sorghum bicolor*) at three spatial scales. *Functional Plant Biology* **35**: 823-836.

Coupel-Ledru A, Lebon É, Christophe A, Doligez A, Cabrera-Bosquet L, Péchier P, Hamard P, This P, Simonneau T. 2014. Genetic variation in a grapevine progeny (*Vitis vinifera* L. cvs Grenache×Syrah) reveals inconsistencies between maintenance of daytime leaf water potential and response of transpiration rate under drought. *Journal of Experimental Botany* **65**: 6205-6218.

Foulkes MJ, Slafer GA, Davies WJ, Berry PM, Sylvester-Bradley R, Martre P, Calderini DF, Griffiths S, Reynolds MP. 2011. Raising yield potential of wheat. III. Optimizing partitioning to grain while maintaining lodging resistance. *Journal of Experimental Botany* **62**: 469-486.

Golzarian MR, Frick RA, Rajendran K, Berger B, Roy S, Tester M, Lun DS. 2011. Accurate inference of shoot biomass from high-throughput images of cereal plants. *Plant Methods* **7**: 2.

Granier C, Aguirrezabal L, Chenu K, Cookson SJ, Dauzat M, Hamard P, Thioux JJ, Rolland G, Bouchier-Combaud S, Lebaudy A, et al. 2006. PHENOPSIS, an automated platform for reproducible phenotyping of plant responses to soil water deficit in *Arabidopsis thaliana* permitted the identification of an accession with low sensitivity to soil water deficit. *New Phytologist* **169**: 623-635.

Greenham K, Lou P, Remsen S, Farid H, McClung C. 2015. TRiP: Tracking Rhythms in Plants, an automated leaf movement analysis program for circadian period estimation. *Plant Methods* **11**: 33.

Hammer GL, Dong Z, McLean G, Doherty A, Messina C, Schusler J, Zinselmeier C, Paszkiewicz S, Cooper M. 2009. Can Changes in Canopy and/or Root System Architecture Explain Historical Maize Yield Trends in the US Corn Belt? *Crop Science* **49**: 299-312.

Hammer GL, Vanderlip RL. 1989. Genotype-by-Environment interaction in grain-sorghum .1. Effects of temperature on radiation use efficiency. *Crop Science* **29**: 370-376.

Hartmann A, Czauderna T, Hoffmann R, Stein N, Schreiber F. 2011. HTPheno: an image analysis pipeline for high-throughput plant phenotyping. *Bmc Bioinformatics* **12**: 148.

Hay JO, Moulia B, Lane B, Freeling M, Silk WK. 2000. Biomechanical analysis of the Rolled (RLD) leaf phenotype of maize. *American Journal of Botany* **87**: 625-633.

Hay RKM, Porter JR. 2006. *The physiology of crop yield*. Oxford: Wiley-Blackwell.

Hui D, Luo Y, Cheng W, Coleman JS, Johnson DW, Sims DA. 2001. Canopy radiation- and water-use efficiencies as affected by elevated [CO_2]. *Global Change Biology* **7**: 75-91.

Koester RP, Nohl BM, Diers BW, Ainsworth EA. 2016. Has photosynthetic capacity increased with 80 years of soybean breeding? An examination of historical soybean cultivars. *Plant, Cell & Environment* **39**: 1058-1067.

Kozai T, Kimura M. 1977. Direct solar light transmission into multi-span greenhouses. *Agricultural Meteorology* **18**: 339-349.

Ku LX, Zhang J, Guo SL, Liu HY, Zhao RF, Chen YH. 2012. Integrated multiple population analysis of leaf architecture traits in maize (*Zea mays* L.). *Journal of Experimental Botany* **63**: 261-274.

Lindquist JL, Arkebauer TJ, Walters DT, Cassman KG, Dobermann A. 2005. Maize radiation use efficiency under optimal growth conditions. *Agronomy Journal* **97**: 72-78.

Long SP, Zhu XG, Naidu SL, Ort DR. 2006. Can improvement in photosynthesis increase crop yields? *Plant Cell and Environment* **29**: 315-330.

Lopez G, Pallas B, Martinez S, Lauri P-É, Regnard J-L, Durel C-É, Costes E. 2015. Genetic Variation of Morphological Traits and Transpiration in an Apple Core Collection under Well-Watered Conditions: Towards the Identification of Morphotypes with High Water Use Efficiency. *PLoS ONE* **10**: e0145540.

Louarn G, Chenu K, Fournier C, Andrieu B, Giauffret C. 2008. Relative contributions of light interception and radiation use efficiency to the reduction of maize productivity under cold temperatures. *Functional Plant Biology* **35**: 885-899.

Malosetti M, Ribaut J-M, van Eeuwijk FA. 2013. The statistical analysis of multi-environment data: modeling genotype-by-environment interaction and its genetic basis. *Frontiers in Physiology* **4**: 44.

Massonnet C, Vile D, Fabre J, Hannah MA, Caldana C, Lisec J, Beemster GTS, Meyer RC, Messerli G, Gronlund JT, et al. 2010. Probing the Reproducibility of Leaf Growth and Molecular Phenotypes: A Comparison of Three Arabidopsis Accessions Cultivated in Ten Laboratories. *Plant Physiology* **152**: 2142-2157.

Mickelson SM, Stuber CS, Senior L, Kaeppler SM. 2002. Quantitative trait loci controlling leaf and tassel traits in a B73 x MO17 population of maize. *Crop Science* **42**: 1902-1909.

Monteith JL. 1977. Climate and efficiency of crop production in britain. *Philosophical Transactions of the Royal Society of London Series B-Biological Sciences* **281**: 277-294.

Moon P, Spencer DE. 1942. Illumination from a non-uniform sky. *Transactions of the Illumination Engineering Society* **37**: 707-726.

Moreau D, Allard V, Gaju O, Le Gouis J, Foulkes MJ, Martre P. 2012. Acclimation of Leaf Nitrogen to Vertical Light Gradient at Anthesis in Wheat Is a Whole-Plant Process That Scales with the Size of the Canopy. *Plant Physiology* **160**: 1479-1490.

Murchie EH, Pinto M, Horton P. 2009. Agriculture and the new challenges for photosynthesis research. *New Phytologist* **181**: 532-552.

Narayanan S, Aiken RM, Vara Prasad PV, Xin Z, Yu J. 2013. Water and Radiation Use Efficiencies in Sorghum. *Agronomy Journal* **105**: 649-656.

Niinemets U, Keenan TF. 2012. Measures of light in studies on light-driven plant plasticity in artificial environments. *Frontiers in Plant Science* **3**: 156.

Otegui ME, Nicolini MG, Ruiz RA, Dodds PA. 1995. Sowing date effects on grain-yield components for different maize genotypes. *Agronomy Journal* **87**: 29-33.

Parent B, Tardieu F. 2014. Can current crop models be used in the phenotyping era for predicting the genetic variability of yield of plants subjected to drought or high temperature? *Journal of Experimental Botany* **65**: 6179-6189.

Parent B, Turc O, Gibon Y, Stitt M, Tardieu F. 2010. Modelling temperature-compensated physiological rates, based on the co-ordination of responses to temperature of developmental processes. *Journal of Experimental Botany* **61**: 2057-2069.

Pound MP, French AP, Murchie EH, Pridmore TP. 2014. Automated Recovery of Three-Dimensional Models of Plant Shoots from Multiple Color Images. *Plant Physiology* **166**: 1688-1698.

Pradal C, Dufour-Kowalski S, Boudon F, Fournier C, Godin C. 2008. OpenAlea: a visual programming and component-based software platform for plant modelling. *Functional Plant Biology* **35**: 751-760.

Pradal C, Fournier C, Valduriez P, Cohen-Boulakia S 2015. OpenAlea: scientific workflows combining data analysis and simulation.In Gupta A, Rathbun S. *Proceedings of the 27th International Conference on Scientific and Statistical Database Management*. La Jolla, California: ACM. 1-6.

Prieto JA, Louarn G, Perez Pena J, Ojeda H, Simonneau T, Lebon E. 2012. A leaf gas exchange model that accounts for intra-canopy variability by considering leaf nitrogen content and local acclimation to radiation in grapevine (*Vitis vinifera* L.). *Plant Cell and Environment* **35**: 1313-1328.

R_Core_Team 2015. R: A Language and Environment for Statistical Computing. 1017. Vienna, Austria. R 3.0.0

Rasband WS 1997-2014. ImageJ, U. S. National Institutes of Health, Bethesda, Maryland, USA, http://imagej.nih.gov/ij/. 298. 1.43m

Rattalino Edreira JI, Otegui ME. 2012. Heat stress in temperate and tropical maize hybrids: Differences in crop growth, biomass partitioning and reserves use. *Field Crops Research* **130**: 87-98.

Reynolds M, Bonnett D, Chapman SC, Furbank RT, Manès Y, Mather DE, Parry MAJ. 2011. Raising yield potential of wheat. I. Overview of a consortium approach and breeding strategies. *Journal of Experimental Botany* **62**: 439-452.

Reynolds M, Foulkes J, Furbank R, Griffiths S, King J, Murchie E, Parry M, Slafer G. 2012. Achieving yield gains in wheat. *Plant Cell and Environment* **35**: 1799-1823.

Sadras VO, Lawson C, Montoro A. 2012. Photosynthetic traits in Australian wheat varieties released between 1958 and 2007. *Field Crops Research* **134**: 19-29.

Sakai H, Hasegawa T, Kobayashi K. 2006. Enhancement of rice canopy carbon gain by elevated CO2 is sensitive to growth stage and leaf nitrogen concentration. *New Phytologist* **170**: 321-332.

Sankaran S, Khot LR, Espinoza CZ, Jarolmasjed S, Sathuvalli VR, Vandemark GJ, Miklas PN, Carter AH, Pumphrey MO, Knowles NR, et al. 2015. Low-altitude, high-resolution aerial imaging systems for row and field crop phenotyping: A review. *European Journal of Agronomy* **70**: 112-123.

Sayre KD, Rajaram S, Fischer RA. 1997. Yield potential progress in short bread wheats in northwest Mexico. *Crop Science* **37**: 36-42.

Sciara G, Salvi S, Cané MA, Welcker C, Cabrera-Bosquet L, Grau A, Bovina R, Tardieu F, Tuberosa R 2015. High-throughput phenotyping of a maize introgression library under water deficit conditions *EPPN Plant Phenotyping Symposium*. Barcelona.

Sinclair TR, Muchow RC. 1999. Radiation use efficiency. *Advances in Agronomy, Vol 65* **65**: 215-265.

Sinclair TR, Shiraiwa T, Hammer GL. 1992. Variation in Crop Radiation-Use Efficiency with Increased Diffuse Radiation. *Crop Science* **32**: 1281.

Sinoquet H, Le Roux X, Adam B, Ameglio T, Daudet FA. 2001. RATP: a model for simulating the spatial distribution of radiation absorption, transpiration and photosynthesis within canopies: application to an isolated tree crown. *Plant Cell and Environment* **24**: 395-406.

Sirault XRR, Condon AG, Wood JT, Farquhar GD, Rebetzke GJ. 2015. "Rolled-upness": phenotyping leaf rolling in cereals using computer vision and functional data analysis approaches. *Plant Methods* **11**: 1-11.

Slattery R, A, Ort D, R. 2015. Photosynthetic energy conversion efficiency: Setting a baseline for gauging future improvements in important food and biofuel crops. *Plant Physiology* **168**: 383-392.

Sommer C, Straehle C, Kothe U, Hamprecht FA 2011. Ilastik: Interactive Learning and Segmentation Toolkit. *8th IEEE International Symposium on Biomedical Imaging*. Chicago, Illinois, USA: IEEE. 230–233.

Song Q, Zhang G, Zhu X-G. 2013. Optimal crop canopy architecture to maximise canopy photosynthetic CO_2 uptake under elevated CO_2 – a theoretical study using a mechanistic model of canopy photosynthesis. *Functional Plant Biology* **40**: 108-124.

Spitters CJT, Toussaint H, Goudriaan J. 1986. Separating the diffuse and direct component of global radiation and its implications for modeling canopy photosynthesis .1. Components of incoming radiation. *Agricultural and Forest Meteorology* **38**: 217-229.

Stanhill G, Fuchs M, Bakker J, Moreshet S. 1973. The radiation balance of a glasshouse rose crop. *Agricultural Meteorology* **11**: 385-404.

Teixeira EI, George M, Herreman T, Brown H, Fletcher A, Chakwizira E, de Ruiter J, Maley S, Noble A. 2014. The impact of water and nitrogen limitation on maize biomass and resource-use efficiencies for radiation, water and nitrogen. *Field Crops Research* **168**: 109-118.

Tian F, Bradbury PJ, Brown PJ, Hung H, Sun Q, Flint-Garcia S, Rocheford TR, McMullen MD, Holland JB, Buckler ES. 2011. Genome-wide association study of leaf architecture in the maize nested association mapping population. *Nature Genetics* **43**: 159-U113.

Zhang TY, Suen CY. 1984. A fast parallel algorithm for thinning digital patterns. *Communications of the Acm* **27**: 236-239.

Zhu X-G, Long SP, Ort DR. 2010. Improving Photosynthetic Efficiency for Greater Yield. *Annual Review of Plant Biology* **61**: 235-261.

Figure Captions

Figure 1. Hemispheric images of the greenhouse seen from below at a given x-y position, superimposed to the sun paths (yellow lines) during (a) winter and (c) summer solstices and (b) spring and (d) autumn equinoxes. Time courses of the fraction of transmitted direct light at three different positions (red, green and black lines) in the greenhouse at four different dates (e-h). Grey dashed lines represent the average greenhouse transmission value. Maps of the fraction of transmitted direct light in the greenhouse at the same dates (i-l). Black, red and green dots represent the three studied positions in the greenhouse. The black arrow represents the geographical North.

Figure 2. Schematic representation of the method for estimating the local PPFD reaching each x-y position in the greenhouse using daily direct light maps (a), a diffuse light map (b) and the local amount of PPFD (direct + diffuse) light map (c).

Figure 3. Comparison of measured and estimated available PPFD. (a) Bar plots represent the comparison between measured and estimated weekly PPFD at each of the six positions in the greenhouse equipped with light sensors. (b) Time courses of measured and estimated PPFD with an hourly basis at the positions of the six light sensors.

Figure 4. Step-by step method to extract mean leaf angles from a multi-view set of *Zea mays* plant images (a), side image selection from top image (b), binarization (c), skeletonization (d), identification of 50-pixel elements and calculation of angles for each element (e,f). The output of calculations is presented for three maize lines with contrasting architectures. (g) Time course of mean leaf angle as a function of thermal time ($d_{20^{o}C}$) after sowing, autumn experiment (h). Values are the mean ± SD of 5 replicates.

Figure 5. Canopy structure *Zea mays* plants in the greenhouse superimposed to a three-dimensional array of voxel 0.20 m × 0.20 m × 0.20 m (a). 3D representation of the grid corresponding to the 1680 plant in the greenhouse (b). Each volume represents a voxel, with a size proportional to the leaf area inside the voxel and a colour representing the dominant leaf angle class. Dark blue 60°, pale blue 53°, green 47°, orange 42°, red 36°.

748 **Figure 6.** 3D representation of 10 contiguous *Zea mays* plants in the greenhouse at 20 (a), 35
749 (b) and 50 (c) days after sowing. (d ,e, f) Bar plots representing daily light interception per
750 plant obtained with the RATP model for the plants depicted in Figures a, b and c.

751 **Figure 7.** Time courses of biomass accumulation (a) and intercepted PPFD (c), and biomass
752 accumulation of *Zea mays* as a function of intercepted PPFD (d) in two experiments in
753 autumn and winter-spring. Insets in panels a, c and e present the comparison of biomass (b),
754 intercepted PPFD (d) and RUE (f) between experiments. Values are the mean ± SD of 115 and
755 92 replicates for autumn and winter experiments, respectively.

756 **Figure 8.** Histograms showing variation in cumulated intercepted PPFD (a) and biomass (b)
757 per plant in *Zea mays* plants growing in Exp 2. The relationship between total intercepted
758 PPFD per plant and total cumulated biomass (c). Red and blue symbols / bars refer to water-
759 deficit and well-watered conditions. Each point represents a plant (n= 1600 (200 genotypes x
760 2 water scenarios x 4 repetitions))

761 **Figure 9.** Relationship between radiation-use efficiency (RUE) and leaf net photosynthesis (a)
762 and leaf stomatal conductance (b) in eight genotypes of *Zea mays* with contrasting RUEs
763 grown under well-water (open symbols) and water-deficit conditions (grey symbols). Each
764 point represents the mean ± SE of 3 replicates.

765

766 Fig. 1

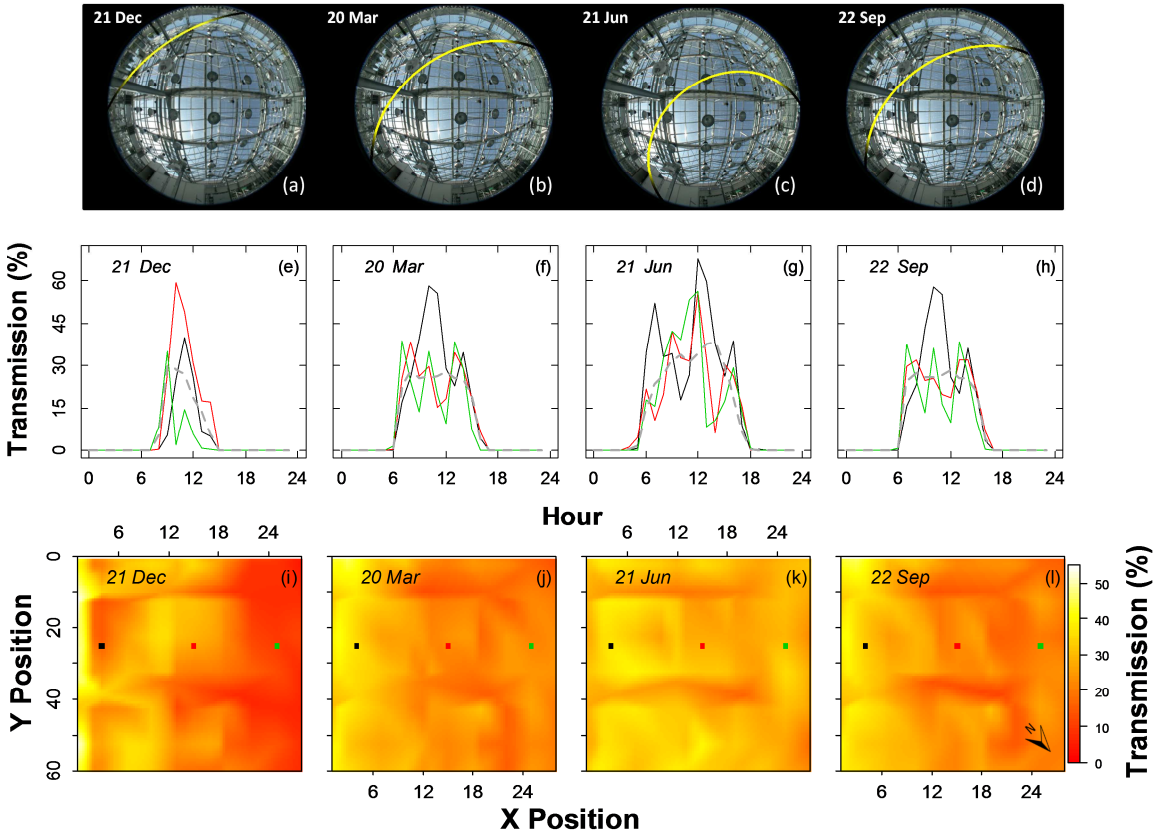

767

768

769

770 Fig. 2

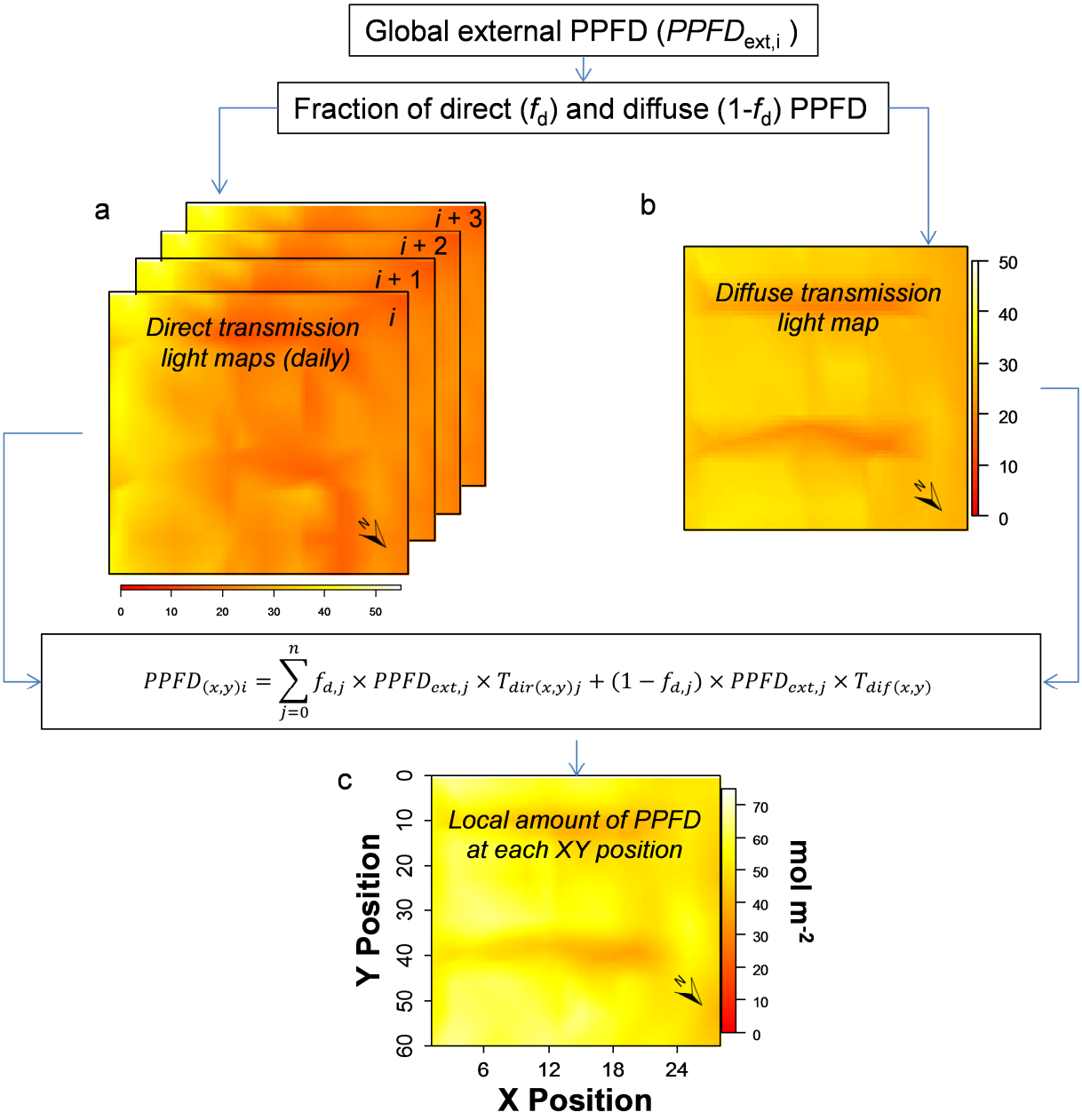

771

772

773

774 Fig. 3

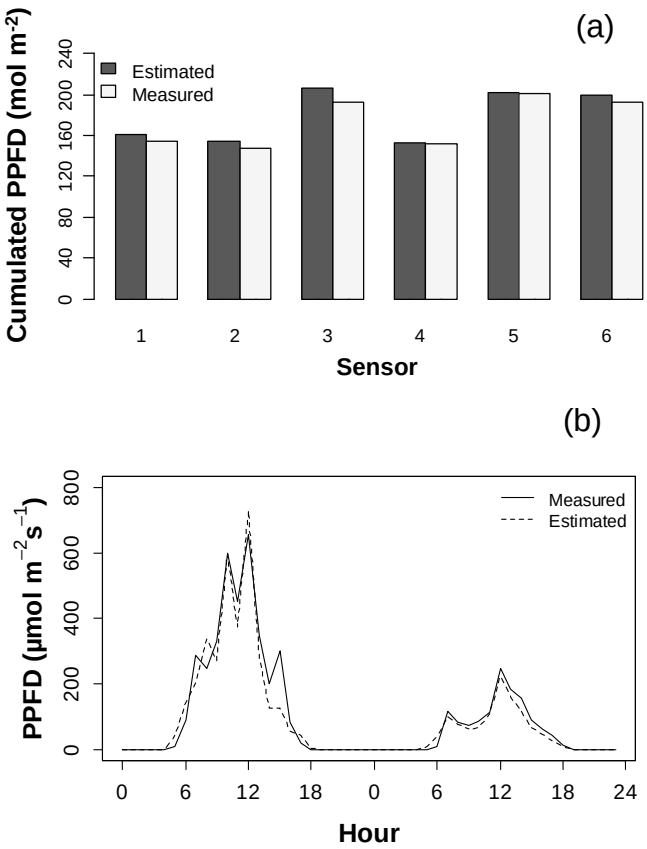

775

776

777 Fig. 4

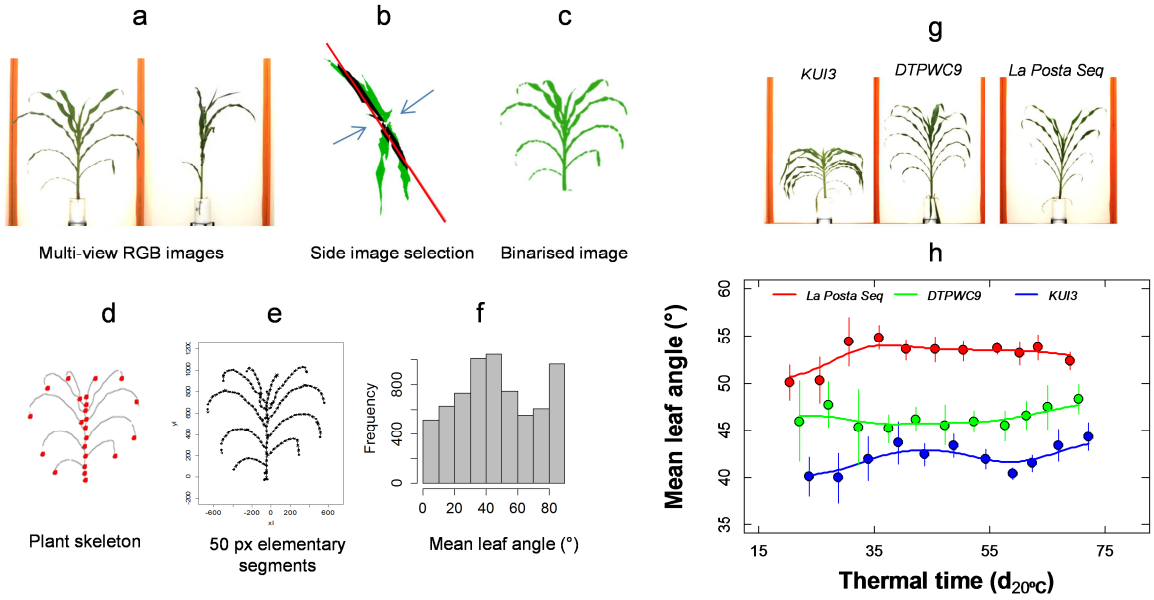

778

779

780 Fig. 5

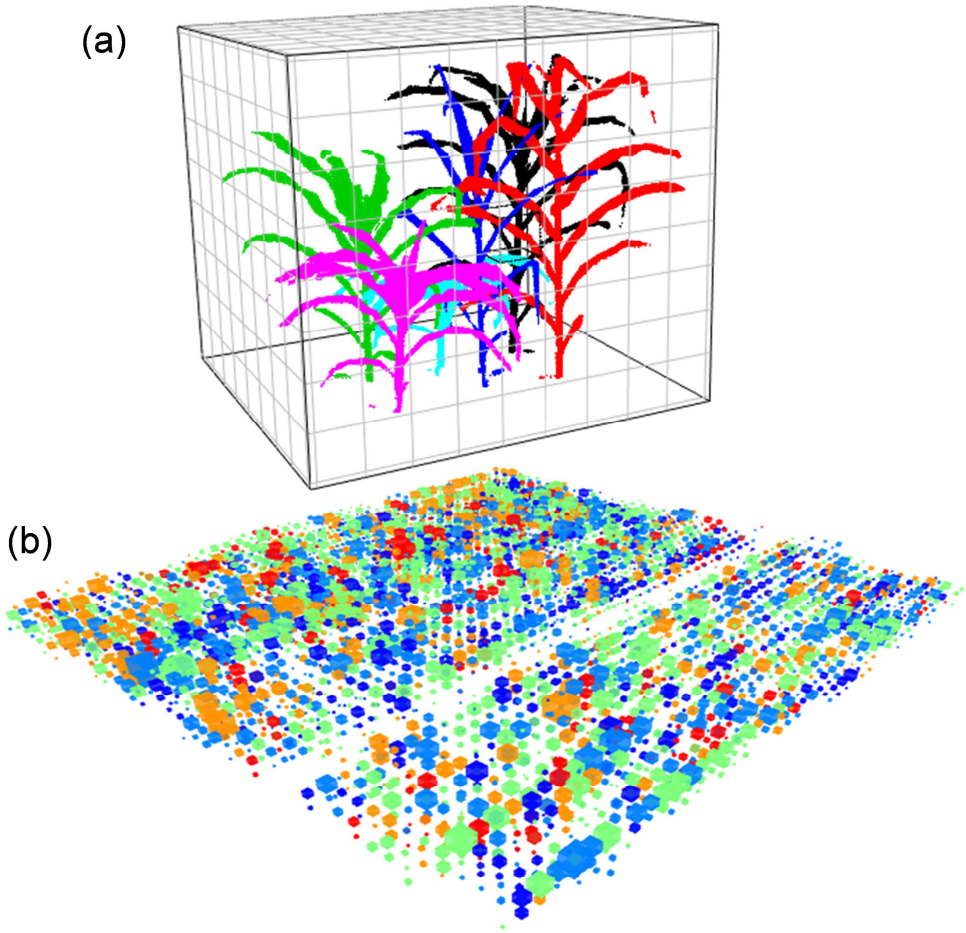

781

782

783 Fig.6

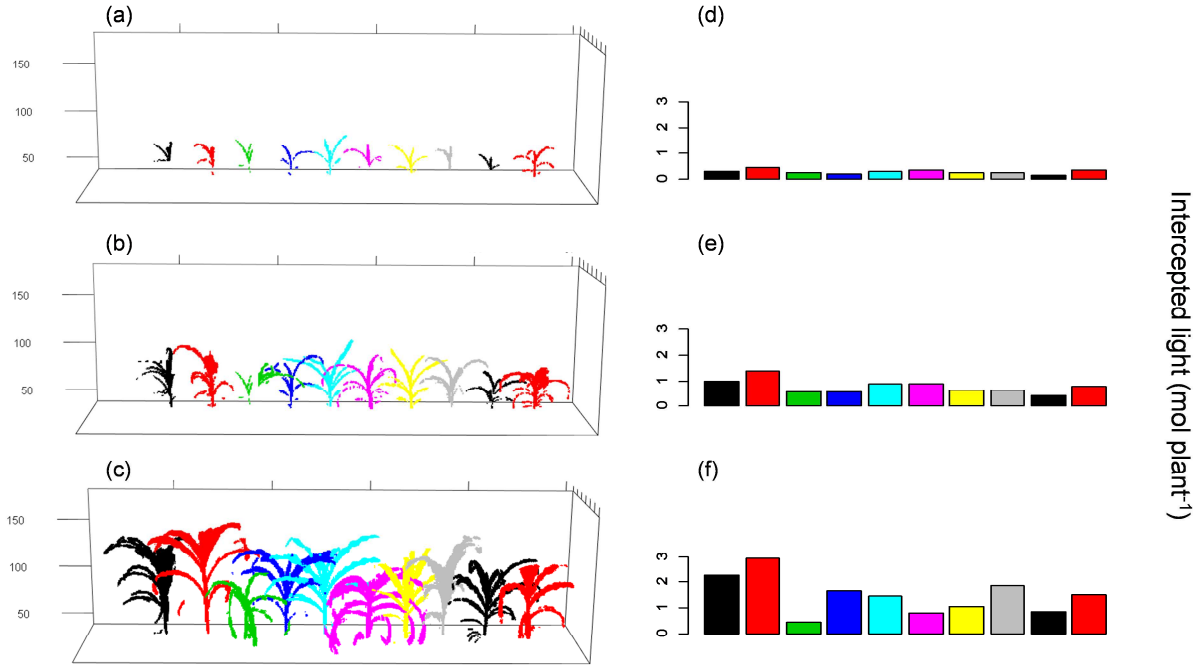

784

785 Fig.7

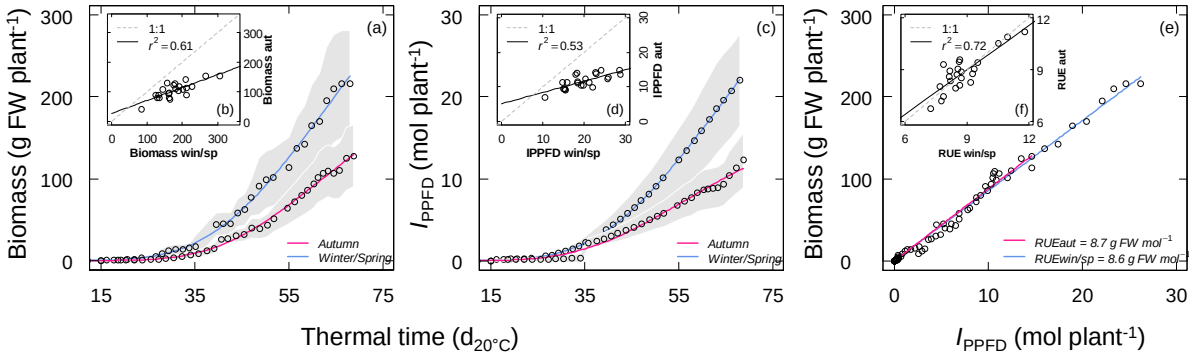
Biomass (g FW plant-1)
(a)
1:1
r2 = 0.61
(b)
Biomass win/sp
Biomass aut
Autumn
Winter/Spring
IPPFD (mol plant-1)
(c)
r2 = 0.53
(d)
IPPFD win/sp
IPPFD aut
(e)
r2 = 0.72
(f)
RUE win/sp
RUE aut
RUEaut = 8.7 g FW mol-1
RUEwin/sp = 8.6 g FW mol-1
Thermal time (d20°C)
IPPFD (mol plant-1)

786

787 Fig.8

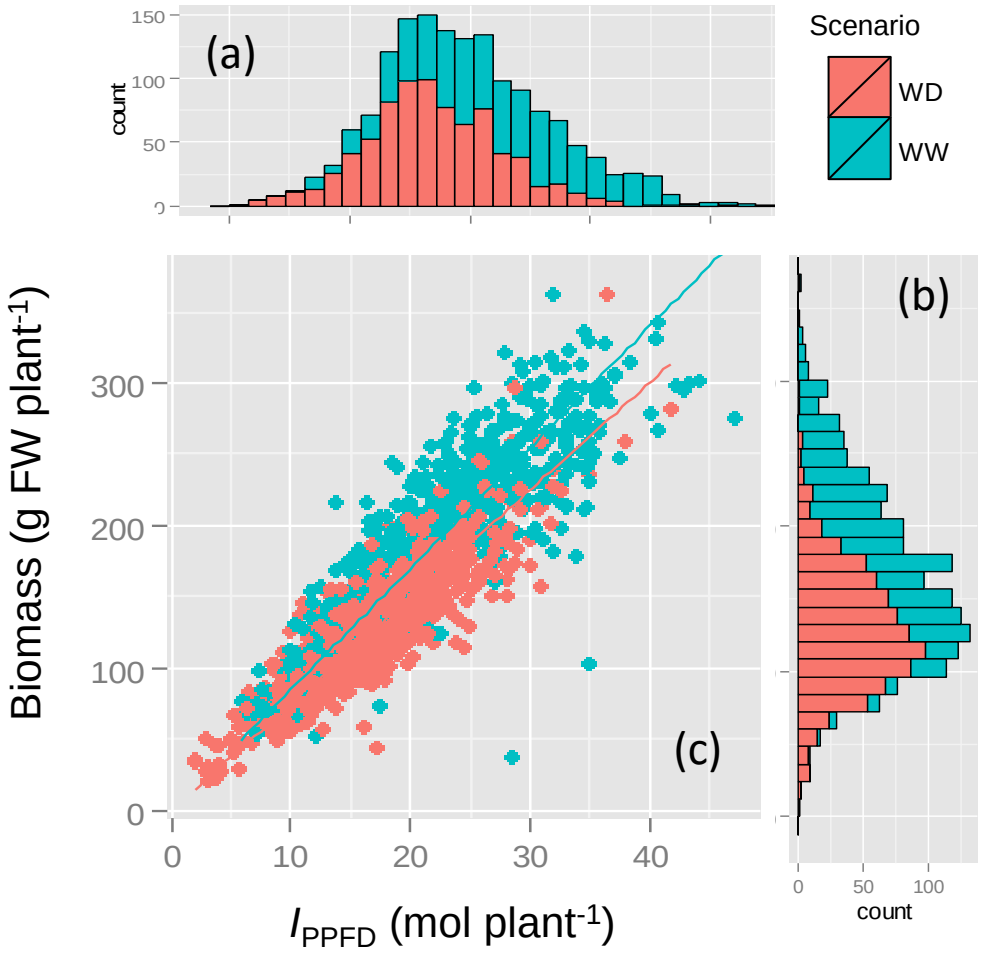
(a)
count
150
100
50
0
Scenario
WD
WW
(b)
0
50
100
count
(c)
Biomass (g FW plant-1)
300
200
100
0
0
10
20
30
40
IPPFD (mol plant-1)

788

789 Fig.9

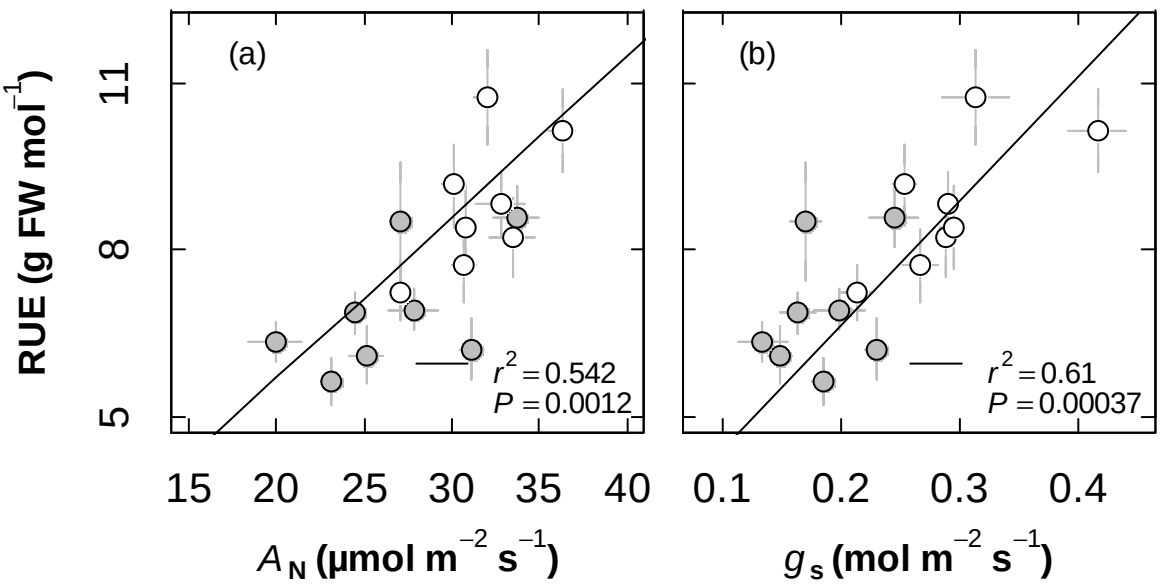

790

791

792

Supporting Information

Additional supporting information may be found in the online version of this article.

Fig. S1. Pipeline analysis of greenhouse hemispherical images.

Fig. S2. Comparison between measured and predicted leaf area and plant biomass.

Methods S1. Shiny App for Sun Paths and Light transmission calculation.

Table S1. Detailed list of software and packages used in this study.

Video S1. Direct light transmission over a year at the different positions in the greenhouse.